Hindawi Publishing Corporation
EURASIP Journal on Image and Video Processing
Volume 2009, Article ID 693274, 9 pages
doi:10.1155/2009/693274

Research Article

Resistivity Probability Tomography Imaging at the Castle of Zena, Italy

Vincenzo Compare,[1] Marilena Cozzolino,[1] Paolo Mauriello,[1] and Domenico Patella[2]

[1] *Department of Science and Technology for Environment and Territory, University of Molise, Via Mazzini 8, 86170 Isernia, Italy*
[2] *Department of Physical Sciences, University Federico II, University Campus of Mt. S. Angelo, 80126 Naples, Italy*

Correspondence should be addressed to Domenico Patella, patella@na.infn.it

Received 27 January 2009; Revised 25 June 2009; Accepted 8 October 2009

Recommended by Anna Tonazzini

We present the results of an electrical resistivity investigation performed at Castle of Zena (Castello di Zena), a 13th-century fortress located between the towns of Fiorenzuola and Piacenza in the Emilia Romagna Region (Northern Italy), in the frame of a project of restoration. Dipole-dipole resistivity tomographies were planned in three areas suspected of containing buried archaeo-architectural remnants. Data analysis has been made using a 3D tomography imaging approach based on the concept of occurrence probability of anomaly sources in the electrical resistivity distribution. The 3D tomography has allowed three interesting anomaly source areas to be identified in the 1-2 m depth range below ground level. Subsequent excavations have brought to light a *giacciara*, that is, a brickwork room for food maintenance, a furnace, and the basement of a wing of the castle destroyed in the 18th century, exactly in correspondence with the anomaly sources detected by the resistivity tomography.

1. Introduction

Geoelectrics is one of the most reliable prospecting tools in the field of Cultural Heritage, thanks to the technological and methodological developments in recent years, which have made it a fast target-oriented method. The electrical resistivity parameter, on which the method is based, has such a large variability so as to allow the great majority of the structures and bodies of archaeologic and architectural interest to be readily distinguished, in principle, from the hosting material. To enhance the resolution power of the method, a great help is provided by the recently developed electrical resistivity tomography (ERT) approach, which involves the acquisition and processing of large datasets.

This paper presents the results of an ERT survey, carried out about the Castle of Zena (Castello di Zena) (Figure 1), which is a fortress located near the village of Carpaneto Piacentino, in the lowland between the towns of Fiorenzuola and Piacenza (Emilia Romagna Region, Italy). The foundation date of the Castle of Zena are still unknown, though the first document attesting its presence dates back to 1216. The whole complex, despite the several repairs which it has been subject to in past ages, still preserves the ancient character of a fortress of square plan, as documented in the drawing of Figure 2, dating back to 1701 and based on a land map of 1591. The southern wing of the building, that is, the right-hand side of the map in Figure 2, is attested to have been demolished in the 18th century, thus leaving the courtyard of the castle partially exposed, as visible in the top picture of Figure 1. On the western front, where the entry is situated, the traces of a drawbridge, replaced afterwards by a bridge in masonry, and the ditch that surrounds the castle are visible in the lower picture of Figure 1.

The ERT survey was planned in the framework of the SOCRATES project, sponsored by institutional subjects and finalised to the study and preservation of the castle and surrounding areas. The ERT survey was addressed to study the nature of the subsoil in three different zones, which the historians involved in the project suspected to contain remnants of great archaeo-architectural interest.

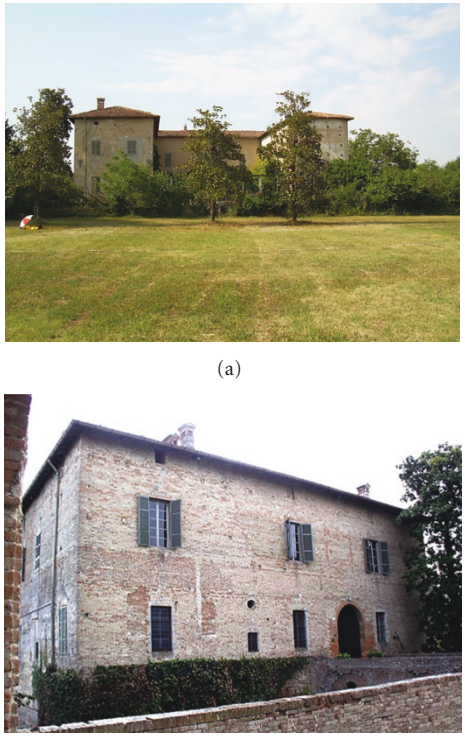

(a) (b)

Figure 1: The Castle of Zena, Carpaneto Piacentino (Emilia Romagna, Italy). Views from the southern (a) and western (b) sides.

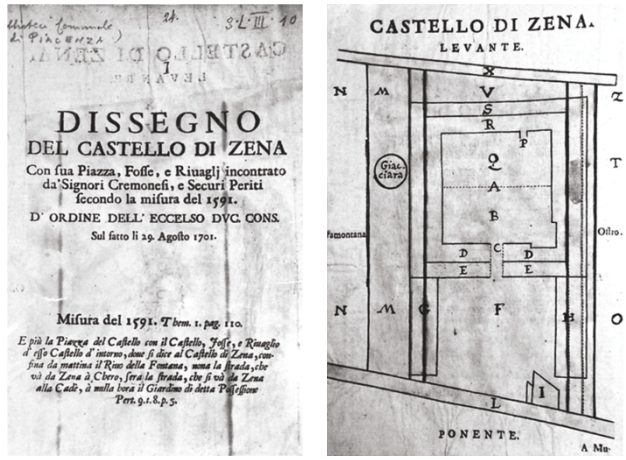

(a) (b)

Figure 2: An archive document from Piacenza dating back to 1701, showing a drawing of the Castle of Zena based on land measurements of 1591.

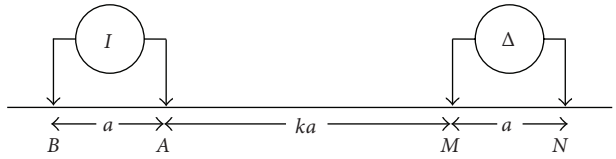

Figure 3: A sketch of the dipole-dipole electrode device for geoelectrical prospecting. A (positive) and B (negative) are the current electrodes to inject a current of intensity I into the ground. M and N are the potential electrodes to measure the voltage $\Delta\phi$. The dipole length is a and $k = 1, 2, \ldots$ determines the spacing between the dipoles as an integer multiple of a.

2. Outline of the Geoelectrical Method

The solution for the electrical potential arising from an electrical current flowing into the ground from a point source of current (a grounded electrode) is the starting theoretical point for the resistivity prospecting method. In practice, there is always a device of four electrodes used to measure the ground resistivity: two are used for injecting a current of intensity I and two for detecting a voltage (potential difference) $\Delta\phi$.

For all of the devices the theoretical solution is basically a superposition of the fundamental equations for the potential from a current point source with appropriate sign for the current. The formulae for evaluating the resistivity of the ground are a product of the impedance $\Delta\phi/I$ and a geometric factor with the units of length which depends on the geometry of the four electrodes. However, as the resistivity is an intrinsic property of a homogeneous material and the subsoil is generally a complex distribution of different materials with different resistivities, the key concept of apparent resistivity, ρ_a, is defined. In simple terms, ρ_a is a volumetric average of a heterogeneous half-space, except that the averaging is not done arithmetically but by a complex weighting function dependent on the 4-electrode device and how it is used.

In near-surface investigations, as in the archaeological prospection, the dipole-dipole (DD) (Figure 3) is the most convenient 4-electrode device, since it provides a very

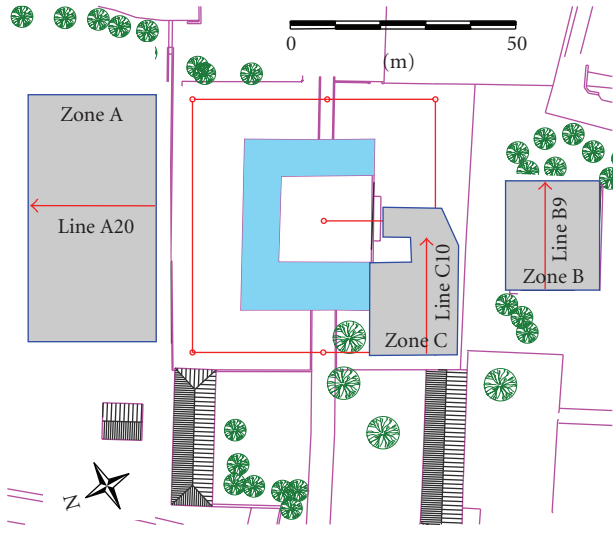

Figure 4: A sketched map of the Castle of Zena (C-shaped central light blue area) and the three ERT A, B, and C survey zones (grey areas). The red lines A20, B9, and C10 are the profiles selected to show examples of the nature of the input data in the form of 2D pseudosections.

Figure 5: A-zone: cropmarks in correspondence with the *giacciara* indicated in the map of Figure 2.

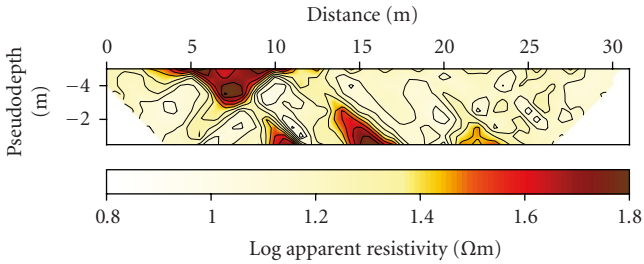

Figure 6: The apparent resistivity pseudosection across the line A20 in the A-zone (red line in Figure 4).

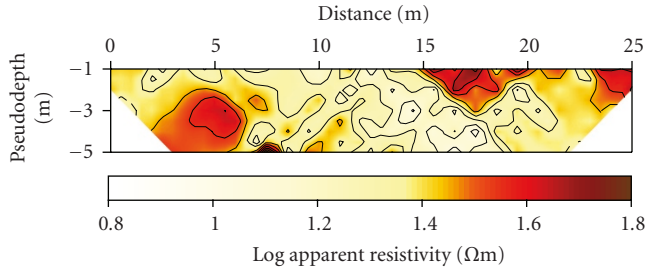

Figure 7: The apparent resistivity pseudosection across the line B9 in the B-zone (red line in Figure 4).

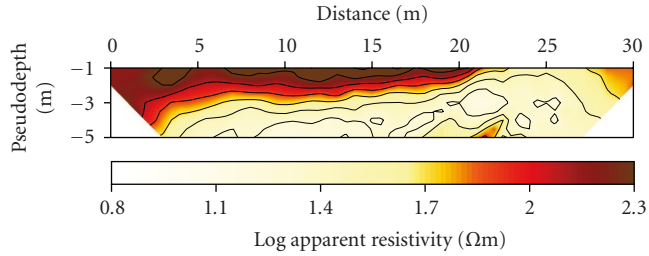

Figure 8: The apparent resistivity pseudosection across the line C10 in the C-zone (red line in Figure 4).

detailed lateral bounding of vertical features. The DD device is normally used in profiling mode to map lateral as well as depth variations of the resistivity. The convention for the DD device shown in Figure 3 is that current and voltage dipole lengths are the same, a, and the spacing between the dipoles is an integer multiple k of a. The DD apparent resistivity is thus given by

$$\rho_a = \pi a k(k+1)(k+2)\frac{\Delta\phi}{I}, \tag{1}$$

and its values are expressed in Ohm·meters (Ωm) in the SI system of units.

To investigate the resistivity distribution along a profile, a $\{\rho_a\}$ dataset is collected from a linear array of dipoles coupled to a transmitter/receiver unit through a series of solid state relays. Measurements are realised from predefined arrays of dipoles selected by the relays.

The plotting convention is to attribute the values of ρ_a at the intersection point of two 45° lines descending from the current dipole and from the voltage dipole. The resulting maps of $\{\rho_a\}$ are contoured at constant (usually logarithmic) intervals. The contoured sections are called pseudosections because they look somewhat like resistivity cross-sections of the ground, but actually they are simply a graphical representation of the $\{\rho_a\}$ dataset. The vertical scale is not depth but some function of the array spacing. For simplest geological models the relative pseudosections do have an intuitive relationship to the actual section but mostly they do not. For a layered earth the contour lines are horizontal and rise and fall in value in the same sense as the actual resistivity, but for the case of even a single vertical contact between dissimilar resistivities the pseudosection is a complex map with no direct relationship to the actual model.

A numerical inversion is used to convert measured apparent resistivity distributed along a pseudosection to electrical resistivity values displayed as a function of depth below surface.

The geoelectric resistivity tomography (ERT) approach comes from taking many ρ_a determinations at as many locations as possible and involves the joint inversion of many independent tests, using an algorithm to discern subtle details from differences which would otherwise not be seen in any one test. The inversion of a $\{\rho_a\}$ dataset collected by the described DD profiling field technique gives rise to a two-dimensional (2D) DD ERT. If one assembles a set of parallel DD profiles, as we did in the Castle of Zena survey, the inversion of the whole $\{\rho_a\}$ dataset provides a three-dimensional (3D) DD ERT.

Resistivity inversion is a typical nonlinear, ill-posed, and underdetermined problem [1–4]. Furthermore, mainly in 3D cases, the number of the model parameters to be inverted is so high that the large computer time required to solve the problem makes the approach almost unpractical in routine applications. An efficient way of dealing with 2D and 3D inversion derives from a linearised form of the nonlinear problem. One-step and iterative linear methods have been proposed; see for example, [5–8]. The main advantage of such methods is that they can greatly reduce the computer time needed to generate an approximate model.

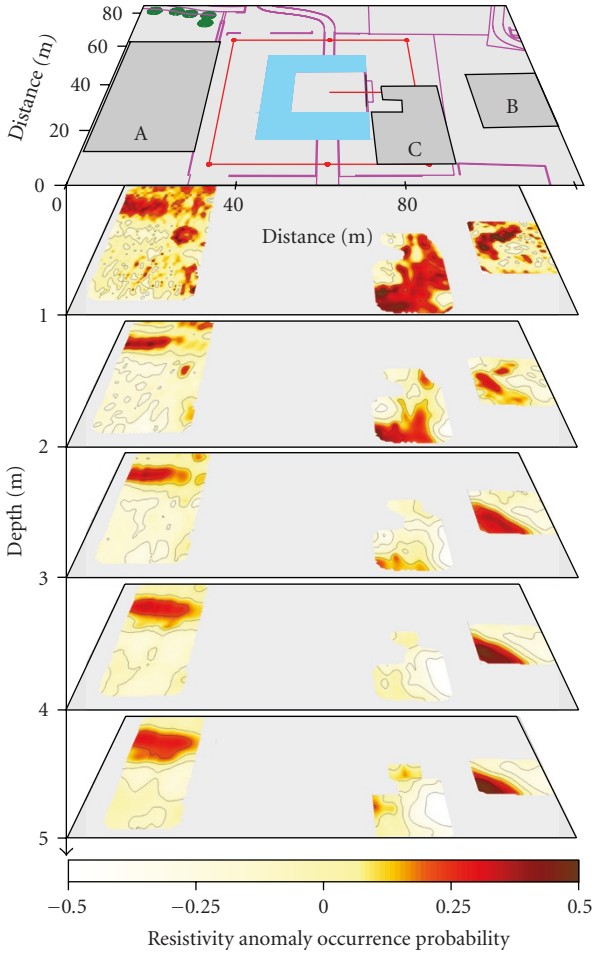

FIGURE 9: The 3D probability tomography in the three surveyed A, B, and C zones of Figure 4, represented with sequences of horizontal slices at increasing depth below the ground surface. The top slice is the reference land map with the three survey zones and the sketched plan of the castle.

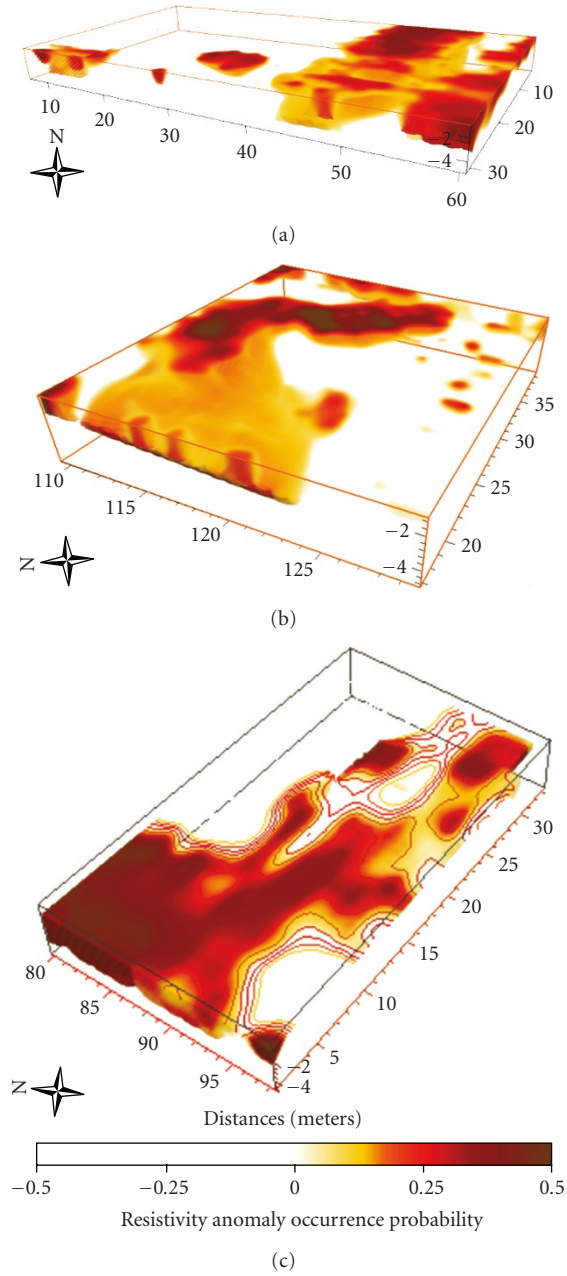

FIGURE 10: 3D views of the probability-based ERT representation in the A-zone (a), B-zone (b), and C-zone (c).

Following the one-step linearised strategy, a probability-based ERT method has also been developed in more recent years as a simple and fast anomaly source imaging tool [9–11]. It has been proven to be very useful in highlighting shape and position of the most probable sources responsible of the ρ_a anomalies detected on the free surface. An outline of the probability-based ERT method is given below, since it was used to interpret the ERT survey performed in the Castle of Zena area.

3. Outline of the Probability Tomography

The probability tomography method consists in the analysis of an occurrence probability function ranging between −1 and +1, defined as a normalised cross-correlation product of the $\{\rho_a\}$ dataset by a suitably digitised scanner function, derived from the electric potential theory by a perturbation technique under Born approximation [10].

In practice, since the source pattern generating the observed anomalies is unknown, an elementary source of unitary strength is ideally used to scan the volume beneath the surveyed area, called the tomospace, and search where the sources are most probably located. From the analytical point of view, this ideal process corresponds to calculating the occurrence probability function in a grid of points in the tomospace. A positive value of this function will give the occurrence probability of an increase of resistivity with respect to a reference resistivity value, whereas a negative value will give the occurrence probability of a decrease of resistivity. By scanning the tomospace, a full 3D image reconstruction of the anomaly sources distribution can at last be obtained in a probabilistic sense.

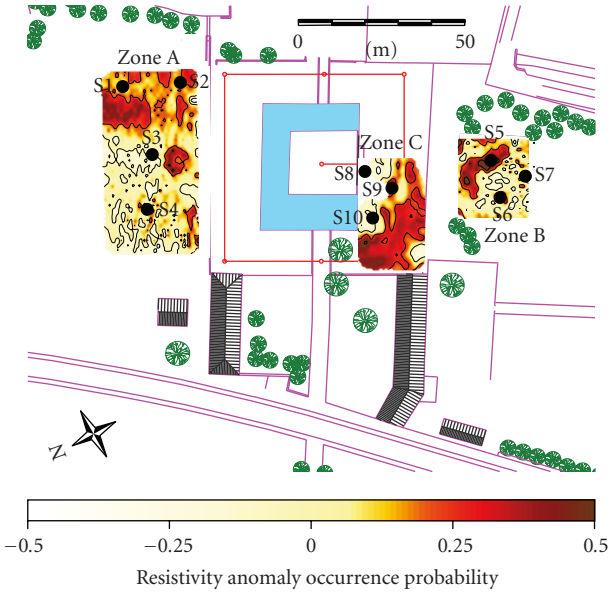

Figure 11: Geoelectrical probability tomography at 1 m of depth b.g.l. and locations of the mechanical surveys S1-S10, indicated by black circlets.

Figure 12: A-Zone: the *giacciara* or icebox found in correspondence of the rounded sequence of nuclei in the probability tomography of Figure 11.

A suitable reference resistivity can be either the true background resistivity, if it is known, or simply the average apparent resistivity, as we did in this study. At the end of the scanning procedure, one can draw sections or, more efficaciously, 3D images of the probability distribution pattern in the tomospace.

Besides this primary scope of the method, worthy of mention is a second, not less important peculiarity, which makes the 3D probability tomography a versatile and objective imaging approach. Since the algorithm can deal even with multiple datasets, independently of the acquisition technique, it also works as an intrinsic filter. The result is a simultaneous smoothing of the uncorrelated noise and suppression of any correlated phantom effects. In principle, this peculiarity derives from the circumstance that such types of disturbances have zero probability to be generated by true anomaly sources within the context of the geoelectrical theory.

Concluding, we think that it is useful to point out that the probability-based ERT approach cannot give estimates of the true resistivity contrasts which characterise the sources of anomalies. Therefore, it appears to be more appropriate in those circumstances in which the resistivity contrast of the targets is either known in advance or relatively less relevant than the discovery of their existence and retrieval of their shape. This is usually the case in target-oriented applications to archaeology. Otherwise, the method can be considered a valuable support to the classical interpretation. Its results can in fact be used as a priori robust geometrical constraints in anyone of the inversion routines.

4. The Survey Planning

As previously anticipated, the ERT survey was carried out by a direct current multielectrode resistivity meter, capable of handling up to 254 electrodes. The DD electrode device was adopted using 1 m long dipoles displaced at a step of 1 m along each profile with k in (1) reaching the maximum value of 10. The following three different zones (Figure 4) were investigated.

Zone A: it is an area of 1674 m^2, located close to the northern side of the fortress, where a car park underground had been planned. 37 parallel profiles, 31 m long and spaced 1.5 m apart, were realised. Each profile consisted of 235 measurements, thus totalling 8695 data points. In this zone, a *giacciara* is indicated with a circle in the old drawing of the fortress, close to its northern wing (Figure 2). The probable presence of the round structure, likely a brickwork room used in the past for the maintenance of food, is also suggested by the cropmarks easily visible on the ground (Figure 5), nearly where it is indicated in the map of Figure 2.

Zone B: it covers an area of 620 m^2, located south of the castle, where the construction of a swimming pool had been planned. 21 parallel profiles, 31 m long and spaced 1 m apart, were investigated. Each profile consisted of 185 measurements, thus totalling 3885 data points.

Zone C: it covers an area of about 600 m^2, located inside the southwestern portion of the ditch that surrounds the fortress, where part of the destroyed southern wing of the castle was founded. Due to logistic difficulties, 18 profiles spaced 1 m apart, but with different lengths ranging between 15 m and 31 m, were measured. The total number of data points was 3560.

Table 1 reports the minimum, maximum, and mean ρ_a values in Ωm obtained in each of the surveyed zones. The mean value in each zone was calculated taking the average of the logarithms of the corresponding ρ_a values.

For the sake of brevity, we show in Figures 6, 7, and 8 only three apparent resistivity pseudosections, one for each zone, in order to give an idea of the nature of the input data. We now proceed directly to the 3D probability tomography approach that we have used to detect and confine the sources of the apparent resistivity anomalies.

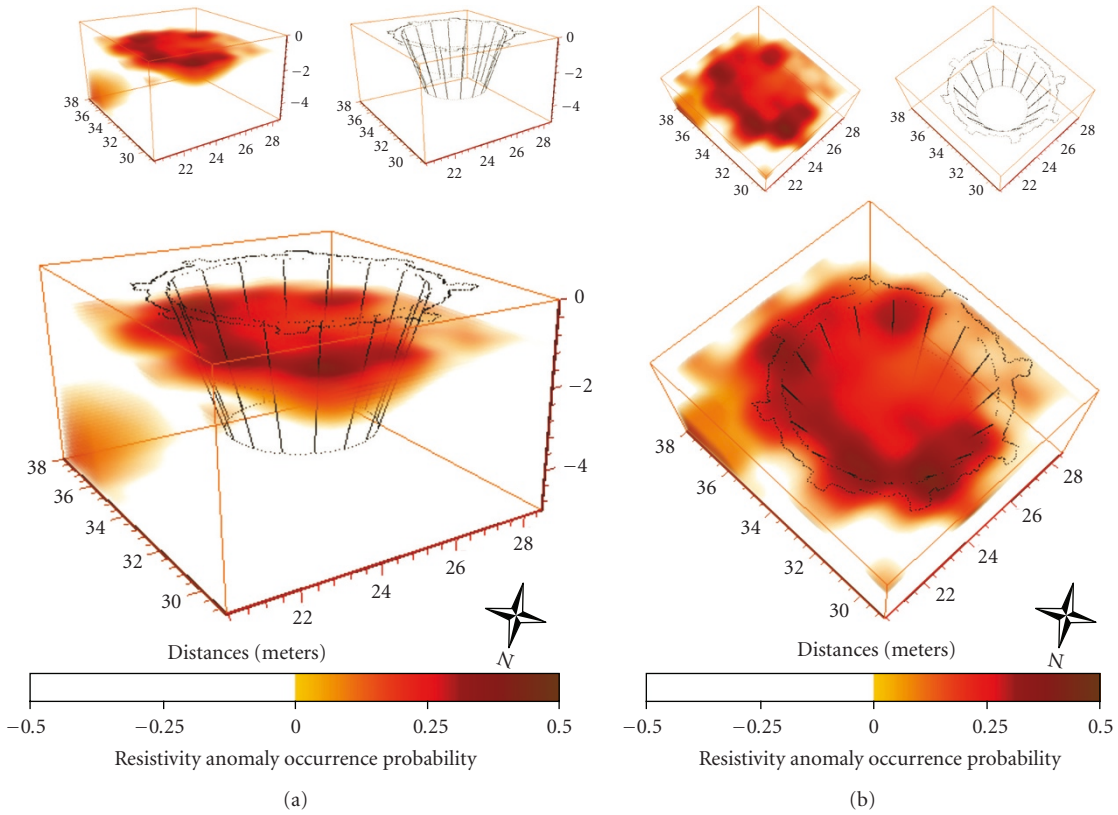

Figure 13: A-Zone: a sketch of the *giacciara* compared with the particular of the round sequence of nuclei extracted from the 3D image of Figure 10(a), from a lateral (a) and a top (b) view.

Table 1: The minimum, maximum, and mean apparent resistivity values in Ωm obtained in the surveyed zones A, B, and C.

Zone	$\rho_{a,\min}$	$\rho_{a,\max}$	$\rho_{a,\text{mean}}$
A	0.67	52367.28	29.92
B	2.94	218.31	24.76
C	3.27	2055.32	87.05

5. The 3D Probability Tomography

Figure 9 shows the results of the 3D probability-based ERT imaging applied to the $\{\rho_a\}$ datasets collected in the three zones marked in Figure 4. In each zone, the number of the model cells used for the 3D ERT imaging is exactly the same as that of the data points. The 3D ERT image consists of a sequence of horizontal slices at increasing depth from 1 m down to 5 m beneath the ground level (b.g.l.). A rather complex pattern of resistivity anomaly sources can readily be observed. The group of sources, deserving to be analysed from the archaeo-architectural point of view, can reasonably be associated with the highs occurring within the first 3 m of depth. These highs, that is, source nuclei characterised by a positive occurrence probability, would indicate the presence of structures with true resistivity higher than the reference uniform resistivity in each zone. The large positive and negative nuclei, centred at a depth not less than 4 m b.g.l. in the B-zone and the C-zone, respectively, and within which the maximum absolute occurrence probabilities have been obtained, may reasonably indicate, instead, the presence of a vertical discontinuity. This discontinuity is assumed to separate two geological media with resistivity on a side higher and on the other side lower than the reference resistivity. The reference resistivity was taken equal to the average apparent resistivity of 29.92 Ωm in the A-zone, 22.80 Ωm in the B-zone, and 87.04 Ωm in the C-zone.

More compact 3D views of the highs of probable archaeo-architectural interest under the surveyed zones are reported separately in Figure 10. In all of these and following 3D views the resistivity anomaly occurrence probability scale has been modified, by compressing the light-to-dark colour sequence entirely within the positive half-scale and leaving colourless the negative half-scale.

Moreover, to help focus the discussion, we consider as a reference map the horizontal slice at 1 m of depth, extracted from Figure 9 and depicted in Figure 11. All of the relative maxima of the highs of probable archaeo-architectural interest are located in this slice, where the sites of 10 holes, bored after the ERT prospecting for ground-truthing, are also indicated. The results of this activity are reported separately for each zone.

5.1. A-Zone. Worthy of note appears the isolated rounded sequence of nuclei visible in Figure 11 at the centre of the

Figure 14: B-zone: the furnace found in correspondence with the longer side of the L-shaped sequence of nuclei in the geoelectrical tomography of Figure 11.

A-zone, close to its right-hand borderline. The location of this source exactly corresponds with the cropmarks visible in Figure 5. The subsequent archaeological excavation allowed a circular structure with radius and height of 3.3 m to be discovered (Figure 12), immediately under the humus [12]. It was found made of pebbles and bricks tied up with a mortar rich in sand in the top portion, made of disjointed bricks and slightly flared at the bottom, and externally surrounded by eight small buttresses, set at a regular distance of about 2.6 m. This regular and well-preserved masonry structure was readily ascribed to the circular plot indicated as *giacciara* in the ancient drawing reported in Figure 2 [12].

For a better appreciation of the resolving power of the exposed probability tomography method, Figure 13 shows a zoom of the 3D image in Figure 10(a), under two different angles of view, limited only to the central round sequence of nuclei. A sketch of the *giacciara* is also plotted at the correct place as from the digging. In both images, the round sequence of nuclei appears to correspond exactly with the trace of the *giacciara* on the horizontal plane through its centre. Furthermore, in the lateral view in Figure 13(a), the full bowl-shaped set of source nuclei appears to smoothly conform to the very regular nest-shaped structure of the *giacciara*.

In the A-zone 4 holes (S1-S4) located as in Figure 11 were also bored. The results from the S2 hole, bored down to 5 m of depth in correspondence with the top right alignment of small positive nuclei, showed the only significant anomalies. In S2, a layer with significant signs of human activity was in fact detected at about 1.65 m of depth. A slimy-sandy-clayey layer, rich of bricks and carbonaceous frustules, was found [13]. This fertile layer has, however, not yet been confirmed by direct archaeological excavations. It may reasonably extend over the whole top third of the A-zone, likely as patches separated by sterile zones. A support to this interpretation derives from the discontinuous nature of the dark nuclei and the circumstance that the hole S1, located a little outside the large horizontal sequence of nuclei in the top left-hand side of the area, did not meet any remnants. No interesting archaeological data came also out of the S3 and the S4 holes, thus confirming the absence of resistivity anomaly source nuclei in those areas.

5.2. B-Zone. An inclined L-shaped sequence of positive nuclei was the only interesting feature appeared in the B-zone, as shown in Figure 11. Three holes (S5-S6-S7) were bored. The S5 hole, located on the longer side of the L-shaped source sequence, revealed, from 0.65 m down to 1.7 m b.g.l., the presence of residues testifying an activity of combustion and/or heating [13]. The first 0.45 m resulted, in fact, to belong to a brick structure, the following 0.15 m to be made of ash and coal and the last 0.45 m of burnt clay. The subsequent digging brought to the light a roofless furnace dating back to the 15th-16th century (Figure 14). The complex presents two anterooms (*prefurni*) and a room of combustion that probably contained part of the last batch of bricks employed for the construction of the castle [12].

The hole S6 was bored down to 5 m of depth, in correspondence with the small positive nucleus located at the centre of the lower half of the zone. The most significant archaeological layer was found between 0.7 and 1.47 m of depth with abundant brick fragments. In particular, the first strata are worthy of note because remnants similar to those found in the S5 hole were detected in the same depth range, allowing for a connection between them. The S7 hole, instead, was bored down to 5 m of depth in an area where the geoelectrical tomography did not put in evidence any relevant positive nucleus. The hole confirmed such a result, since only very rare fragments were there detected [13].

As before, a zoom of the 3D image in Figure 10(b), under two different angles of view, limited only to the portion of the longer side of the L-shaped sequence, where the nuclei with highest occurrence probability were found, is depicted. A sketch of the furnace is also plotted at the correct place as inferred from the digging. In both 3D images, it can readily be observed that the selected portion of the L-shaped set of nuclei exactly corresponds with the trace of the discovered furnace on the horizontal plane through its floor. Moreover, the top view in Figure 15(b) shows that the sequence of the small nuclei closely conforms to the disposition and shape of the discovered rooms.

5.3. C-Zone. The C-zone is almost totally dominated by a positive pattern of source occurrence probabilities, composed of a double set of parallel positive nuclei, which appear to conform at right angle to the southwestern corner of the castle. The internal sequence of nuclei may reasonably attest the presence underground of the foundations of the fourth wing, including the tower, as indicated in the drawing of Figure 2, both destroyed in the 18th century. The outer sequence of positive nuclei may, instead, be associated to

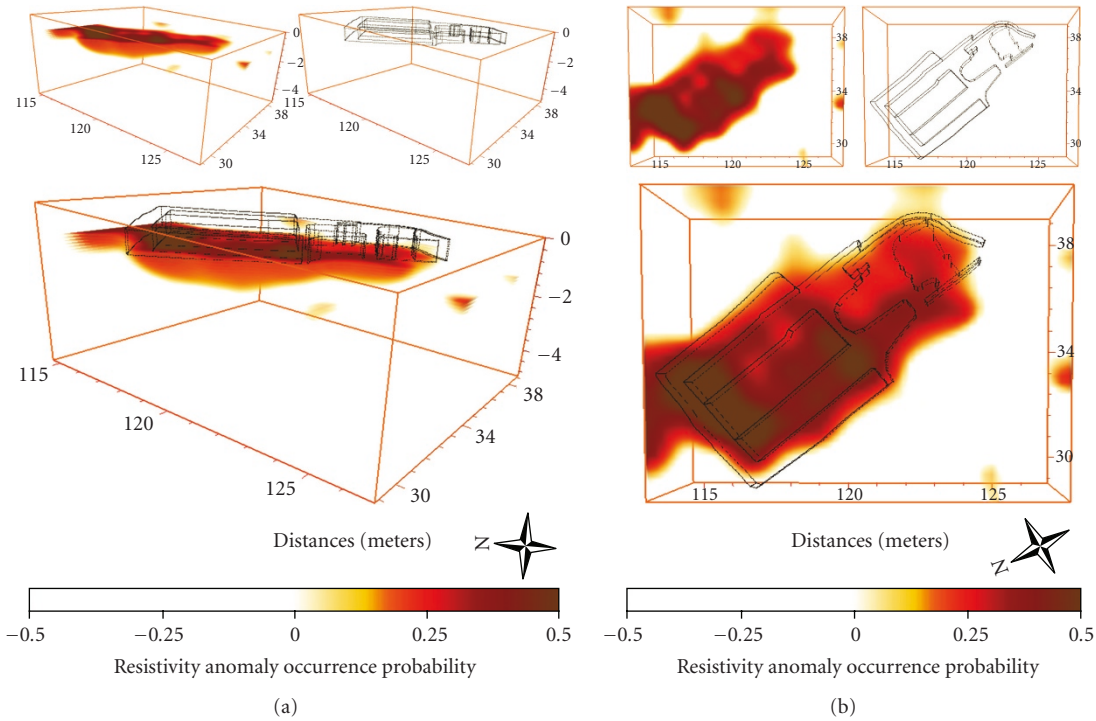

Figure 15: B-Zone: a sketch of the furnace compared with the last portion of the longer side of the L-shaped sequence of nuclei extracted from the 3D image of Figure 10(b), from a lateral (a) and a top (b) view.

Figure 16: C-zone: a nearly east-westward view of the foundations of the fourth wing of the Castle of Zena found in correspondence of the inner sequence of nuclei at right angle in the geoelectrical tomography of Figure 11.

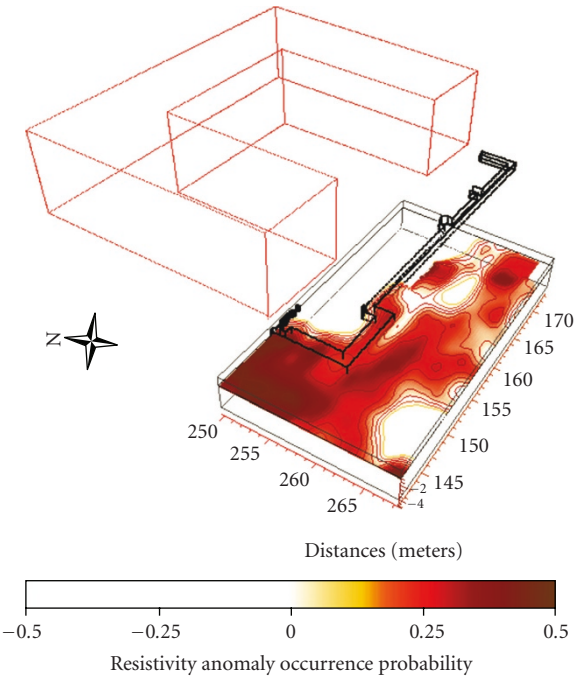

Figure 17: C-Zone: a sketch of the foundations of the destroyed fourth wing and southwestern tower of the castle compared with the inner sequence of the resistivity anomaly source nuclei, replicated from Figure 10(c). The present outline of the castle is drawn on top.

traces of structural elements connected to the castle, likely the base of the former embankment of the ancient ditch.

In the C-zone three holes were bored. The hole S8 was bored down to the depth of 4 m outside the area surveyed by the ERT. At 1.75 m of depth, a compacted gravel layer was found with traces of mortar, probably constituting the

allurement layer of the fourth wing [13]. The hole S9 was bored down to the depth of about 2.5 m in the area of the old ditch now turned into orchard. Bricks were found from 0.97 m down to 1.10 m. Finally, the hole S10 of 4.5 m of depth did not reveal any elements referable to the destroyed wing, but only levels related to the depositional activity in the ditch [13], thus confirming the absence of positive anomaly source nuclei in the ERT of that sector of the C-zone. The subsequent archaeological excavations (Figure 16) brought to light the existence of the foundations of the collapsed southern wing of the castle and the tower at the southwestern corner [12]. Also in this case, in order to evaluate the resolving power of the 3D tomography reconstruction, the 3D tomography image in Figure 10(c) is replicated in Figure 17 for a comparison with the plotted sketch of the foundations as discovered by the digging.

6. Conclusion

We have shown the results from an application of the 3D probability-based ERT imaging approach to a case-study of great importance from both the historical and architectural points of view, consisting in the mapping of some structural remains of the medieval Castle of Zena in three adjacent areas destined to restoration and renovation.

As outlined in previous applications [14, 15], the 3D probability-based ERT method can be considered a self-sufficient procedure, useful to delineate location and shape of the most probable sources of the anomalies detected on the ground surface. In this study, and more generally in the field of Cultural Heritage, the exact knowledge of the true resistivity is not so essential as the location and shape delineation of the expected targets. The rationale for this assumption is that, generally speaking, buried stone remnants or metal bodies of archaeo-architectural interest are characterised by true resistivities higher or lower, respectively, than the resistivity of the hosting environment, which normally consists of medium-to-low resistivity sediments. This, of course, facilitates the detection of meaningful anomalies on the measurement surface. It must also be stressed that the knowledge of the resistivity of the targets generally does not give any added value to the immediate interest of the historians, archaeologists, or architects. This is the reason why the 3D probability tomography approach has not required in this application a further step, aimed at associating true resistivity values to the revealed anomaly sources.

The subsequent ground-truth excavations are to be considered a further successful confirmation of the full validity of the 3D probability-based ERT imaging in detecting the targets location underground and of its resolving power. For a more detailed discussion on this aspect and examples of comparison with the results of inversion-based ERT approaches, the reader is referred to [9, 14, 15].

Acknowledgments

The authors wish to thank for the fruitful collaboration the Archaeology Service of Parma and Piacenza and the Institute of Technologies for Cultural Heritage, National Research Council (CNR), Italy. Thanks are also to Dr. P. Mancioppi, GEONORD Company, Piacenza, Italy, who has kindly provided them with the stratigraphic results from the boreholes, and to Professor. A. Augenti and his group, Department of Archaeology, Ravenna branch, University of Bologna, Italy, who has supervised the archaeological excavations in the areas indicated by the geoelectrical probability tomography.

References

[1] Y. Sasaki, "3-D resistivity inversion using a subspace method," *Geophysical Exploration*, vol. 59, no. 5, pp. 425–430, 2006.

[2] T. Ha, S. Pyun, and C. Shin, "Efficient electric resistivity inversion using adjoint state of mixed finite-element method for Poisson's equation," *Journal of Computational Physics*, vol. 214, no. 1, pp. 171–186, 2006.

[3] A. Pidlisecky, E. Haber, and R. Knight, "RESINVM3D: a 3D resistivity inversion package," *Geophysics*, vol. 72, no. 2, pp. H1–H10, 2007.

[4] L. Marescot, S. P. Lopes, S. Rigobert, and A. G. Green, "Nonlinear inversion of geoelectric data acquired across 3D objects using a finite-element approach," *Geophysics*, vol. 73, no. 3, pp. F121–F133, 2008.

[5] R. Barker, "A simple algorithm for electrical imaging of the subsurface," *First Break*, vol. 10, no. 2, pp. 53–62, 1992.

[6] M. H. Loke and R. D. Barker, "Rapid least-squares inversion of apparent resistivity pseudosections by a quasi-Newton method," *Geophysical Prospecting*, vol. 44, no. 1, pp. 131–152, 1996.

[7] S. Narayan, M. B. Dusseault, and D. C. Nobes, "Inversion techniques applied to resistivity inverse problems," *Inverse Problems*, vol. 10, no. 3, pp. 669–686, 1994.

[8] R. K. Chunduru, M. K. Sen, and P. L. Stoffa, "2-D resistivity inversion using spline parameterization and simulated annealing," *Geophysics*, vol. 61, no. 1, pp. 151–161, 1996.

[9] P. Mauriello, D. Monna, and D. Patella, "3D geoelectrical tomography and archaeological applications," *Geophysical Prospecting*, vol. 46, no. 5, pp. 543–570, 1998.

[10] P. Mauriello and D. Patella, "Resistivity anomaly imaging by probability tomography," *Geophysical Prospecting*, vol. 47, no. 3, pp. 411–429, 1999.

[11] P. Mauriello and D. Patella, "Imaging 3D structures by resistivity probability tomography," in *Proceedings of the 61st EAGE Conference and Technical Exhibition*, Helsinki, Finland, June 1999.

[12] M. Bondi, M. Cavallazzi, and G. Musina, "Progetto di recu-pero e valorizzazione del Castello di Zena e delle sue perti-nenze," Campagna di scavo, 2006, http://www.castellodizena.it/index.php/it/castello.

[13] F. Boschi, "Progetto di recupero e valorizzazione del Castello di Zena e delle sue pertinenze," Campagna di sondaggi meccanici, 2006, http://www.castellodizena.it/index.php/it/castello.

[14] R. Alaia, D. Patella, and P. Mauriello, "Application of geoelectrical 3D probability tomography in a test-site of the archaeological park of Pompei (Naples, Italy)," *Journal of Geophysics and Engineering*, vol. 5, no. 1, pp. 67–76, 2008.

[15] V. Compare, M. Cozzolino, P. Mauriello, and D. Patella, "Three-dimensional resistivity probability tomography at the prehistoric site of Grotta Reali (Molise, Italy)," *Archaeological Prospection*, vol. 16, no. 1, pp. 53–63, 2009.